A Grid-Tied Reconfigurable Battery Storage System

Fa Chen, Hongmei Wang, Wei Qiao, and Liyan Qu
Power and Energy Systems Laboratory
Department of Electrical and Computer Engineering
University of Nebraska–Lincoln
Lincoln, NE, 68588-0511 USA
fa.chen@huskers.unl.edu; hongmei.wang@huskers.unl.edu; wqiao3@unl.edu; lqu2@unl.edu

***Abstract*—This paper presents a grid-tied reconfigurable battery storage system, which consists of a single-phase two-stage bidirectional PWM converter and a reconfigurable battery pack (RBP). The two-stage PWM converter provides an interface between the AC power grid and the RBP and operates in two different modes: (1) grid to battery (G2B) mode, in which the RBP is charged from the AC power grid; and (2) battery to grid (B2G) mode, in which the RBP delivers the stored energy to the grid. In the RBP, fault tolerance and state of charge (SOC) equalization among battery cells can be realized by dynamically configuring the connections of battery cells, no additional SOC equalization circuit is required. A laboratory prototype of the proposed battery system was designed and fabricated. Experimental results on the prototype are provided to validate the features of the proposed battery system.**

Keywords—Fault tolerance; grid-tied converter; reconfigurable battery system; state of charge (SOC) equalization.

I. INTRODUCTION

Rechargeable battery systems have been widely applied in electric vehicles, microgrids, renewable energy storage, home appliances, etc. [1]-[14] Multiple battery cells are connected in series and/or parallel to comprise the battery systems used in these applications to satisfy the voltage, current, and capacity requirements. However, the mismatch of battery cells inside the battery packs, such as different impedances, capacities, aging processes, self-discharging rates, etc., will lead to state of charge (SOC) imbalance among individual battery cells during the repeated charging/discharging operations. To mitigate the impact of SOC imbalance, equalization circuits are commonly used for the battery systems with battery cells connected in series to balance their SOCs [17], [18]. However, the use of an additional equalization circuit increases the cost, complexity, and energy loss of the battery system.

Distributed battery systems consisting of multiple battery units connected in parallel and/or series to form a DC bus are presented in [19]-[23]. Each unit is composed of a battery cell and a bidirectional DC/DC converter, which controls the battery cell independently. Thus, overcharge or overdischarge could be avoided. However, a huge number of DC/DC converters are required as the number of the battery cells increases, which increases the cost, volume, and power loss of the battery system. References [24]-[27] introduce another kind of battery system based on multilevel converters, which generate staircase output waveforms with lower total harmonic distortions (THDs), device stress, and instantaneous rate of voltage change dv/dt. For those battery systems using multilevel converters, each H-bridge or half-bridge submodule was used to control a battery cell separately to realize SOC balance in both charge and discharge operations.

This paper proposes a grid-tied reconfigurable battery storage system, which consists of a single-phase two-stage bidirectional PWM converter and a reconfigurable battery pack (RBP). The two-stage converter consists of a full-bridge converter and a buck-boost bidirectional DC-DC converter. The full-bridge converter works as a power factor correction (PFC) boost converter in the grid to battery (G2B) mode to achieve an AC-DC power conversion and as a buck inverter in the battery to grid (B2G) mode to achieve a DC-AC power conversion. The bidirectional DC-DC converter is used to regulate the charging voltage and current of the RBP in the G2B mode and to provide the desired DC-link voltage in the B2G mode. The reconfigurable design of the RBP has the inherent features of high reliability and fault-tolerant capability. In case one or multiple cells fail, the faulty cell(s) can be quickly disconnected from the battery system by a proper control action without interrupting the operation of the system. In the proposed system, the SOCs of different battery cells can be balanced by properly controlling each individual cell in the G2B and B2G modes. A laboratory prototype of the proposed battery storage system is constructed. Experimental studies are carried out on the prototype to validate the proposed battery storage system.

II. SYSTEM CONFIGURATION AND OPERATION PRINCIPLE

The proposed grid-tied reconfigurable battery storage system is shown in Fig. 1, in which the first stage AC-DC full-bridge converter and the second stage buck-boost DC-DC converter form a two-stage bidirectional PWM converter. The battery system has two operation modes: the G2B mode and the B2G mode. The operation of the system in each mode is explained in the following subsections.

A. G2B Mode

In this operation mode, the full-bridge converter operates as a PFC boost rectifier to realize a high power-factor and a low THD as well as to provide the required DC-link voltage. The DC-DC converter operates as a buck converter to provide the required charging current and voltage for the battery pack.

1) Full-Bridge Converter

In the G2B mode, the full-bridge converter works as a PFC boost rectifier for AC-DC power conversion. There are two switching patterns during the positive half cycle of the AC

This work was supported in part by the U.S. National Science Foundation under Grant IIP-1414393.

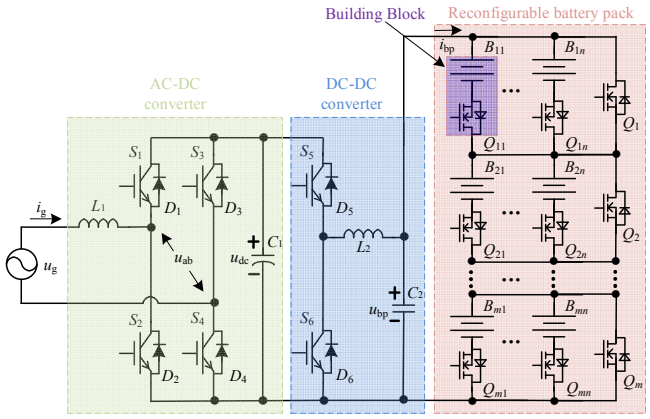

Fig. 1. Proposed grid-tied reconfigurable battery storage system.

grid voltage. In the first switching pattern, the inductor L_1, the device S_2, and the diode D_4 form a boost converter. Only one device S_2 is switched on/off with at a high frequency to shape the input AC current into a sinusoidal waveform that is in phase with the grid voltage. When the device S_2 is turned on, it conducts current with the diode D_4. When the device S_2 is turned off, the current freewheels through the diodes D_1 and D_4. In the second switching pattern, the inductor L_1, the device S_3, and the diode D_1 form another boost converter. Only one device S_3 is switched at a high frequency. When the device S_3 is turned on, it conducts current with the diode D_1. When the device S_3 is turned off, the current freewheels through the diodes D_1 and D_4. Since the two switching patterns are equivalent to generate the same terminal voltage u_{ab}, one of the two patterns could be selected to implement in a PWM period. Similarly, there are two similar switching patterns during the negative half cycle of the AC grid voltage. In each switching pattern, only one of the four devices operates in a switching frequency, leading to a reduced switching loss compared to the unipolar modulation with two devices and the bipolar modulation with four devices operating in a switching period for the full-bridge converter [29], [29].

2) DC-DC Converter

In the G2B mode, the DC-link voltage u_{dc} is higher than that of the battery pack; and the DC-DC converter operates as a buck converter in which only one device S_5 is switched on/off at a high frequency while the device S_6 is always off. Usually, a battery pack is charged with a constant current (CC) constant voltage (CV) method. In the CCCV method, the battery pack is first charged with a CC until it reaches the recommended maximum voltage and then charged with a CV; and the DC-DC converter is necessary to regulate the battery charging current and voltage because the voltage of the battery pack varies when it is in charge or some battery cells fail.

3) RBP

The RBP uses a modular switching circuit with $m \times (n+1)$ controllable switches to manage $m \times n$ battery cells [30]. Each battery cell uses only one controllable switch, e.g., the switch Q_{ij} for the battery cell B_{ij} ($i = 1, \cdots, m$ and $j = 1, \cdots, n$), which turns on/off alternately to connect/cut off the battery cell from the RBP. Each switch and the corresponding battery cell form a building block for the RBP, as shown in Fig. 1, which can be easily plugged in/out for maintenance. In the RBP, n building blocks are connected in parallel to form a battery bank to provide a desired current; m battery banks are connected in series to provide a desired voltage at the terminals of the RBP; and an additional controllable switch Q_i ($i = 1, \cdots, m$) is placed in parallel with each battery bank. When a certain number of building blocks in the ith bank fail such that the bank cannot be charged with the required current, the bank will be bypassed by turning on the switch Q_i, which will provide a path of current flow for the battery cells $B_{(i+1)1}, \cdots, B_{(i+1)n}, \cdots, B_{m1}, \cdots, B_{mn}$ in the lower banks. Otherwise, even if some of the building blocks in the ith bank fail but the remaining building blocks can still be charged with the required current, the switch Q_i will turn off.

In the G2B mode, the battery management system (BMS) monitors the voltage, current, temperature, and SOC of each cell. If any battery cell has an abnormal condition, such as overvoltage, overcurrent, overtemperature, overcharge, overdischarge, etc., it will be disconnected from the system immediately. The remaining cells can still be charged to store energy. The SOC of a battery bank is the average SOC of all the cells in the bank. If a cell is cut off, then its SOC is zero. The SOCs of the available banks are calculated. All of the available banks are charged at first. When the SOC of a bank reaches the maximum value allowed, the bank will be bypassed by turning off all the switches within the bank and turning on the corresponding switch in parallel with the bank. Finally, all of the available banks will be charged and their SOCs will be balanced. Although the RBP is illustrated for cell-level implementation, it is also applicable to module-level implementation by replacing each battery cell in Fig. 1 with a battery module that consists of multiple cells connected in series and/or parallel.

B. B2G Mode

In the B2G mode, the two-stage PWM converter sends the energy stored in the RBP back to the AC power grid. The full-bridge converter operates as a buck inverter for DC-AC power conversion and the DC-DC converter operates as a boost converter to provide the required DC-link voltage for the full-bridge converter.

1) Full-Bridge Converter

In the B2G mode, the full-bridge converter works as a buck inverter for DC-AC power conversion. There are two switching patterns during the positive half cycle of the AC grid voltage. In the first switching pattern, the inductor L_1, the devices S_1 and S_4, and the diode D_2 form a buck converter. Only one device S_1 is switched on/off at a high frequency to shape the input AC current into a sinusoidal waveform that is out of phase with the grid voltage. When the device S_1 is turned on, it conducts current with the device S_4. When the device S_1 is turned off, the current freewheels through the device S_4 and diode D_2. In the second switching pattern, the inductor L_1, the devices S_1 and S_4, and the diode D_3 form another buck converter. Only one device S_4 is switched on/off at a high frequency. When the device S_4 is turned on, it conducts current with the device S_1. When the device S_4 is turned off, the current freewheels through the device S_1 and

diode D_3. Since the two switching patterns are equivalent to generate the same terminal voltage u_{ab}, one of the two patterns could be selected to implement in a PWM period. Similarly, there are two similar switching patterns during the negative half cycle of the AC grid voltage. In each switching pattern, only one of the four devices is switched on/off at a high frequency, leading to a reduced switching loss compared to the unipolar modulation with two devices and the bipolar modulation with four devices operating with a high switching frequency for the full-bridge converter.

2) DC-DC Converter

In the B2G mode, the DC-link voltage u_{dc} is higher than that of the battery pack; and the DC-DC converter operates as a boost converter in which only one device S_6 is switched on/off at a high frequency while the device S_5 is always off with the antiparallel diode D_5 of the device S_5 to provide the conducting path. The battery pack is discharged. The DC-DC converter is necessary to regulate the DC-link voltage by controlling the battery discharging current and voltage because the voltage of the battery pack varies when it is in discharge or some of the battery cells fail.

3) RBP

All of the available banks are discharged at first. When the SOC of a bank reaches the allowed minimum value, it will be bypassed by turning off all the switches within the bank and turning on the corresponding switch in parallel with the bank. Finally, all of the available banks will be discharged and their SOCs will be balanced.

III. Control Sshemes for the Battery System

Since the control schemes of the proposed grid-tied reconfigurable battery system operated in the G2B mode and the B2G mode are different, they are introduced separately in this section.

A. G2B Mode

1) Control of Full-Bridge Converter

In the G2B mode, a dual-closed-loop control scheme is designed for the bidirectional full-bridge converter. The outer control loop is utilized to regulate the DC-link voltage while the inner control loop is used to shape the input current, as shown in Fig. 2, where u_{dc}^* is the DC-link voltage command, u_{dc} is the measured DC-link voltage, i_g^* is the AC grid current command, and i_g is the measured grid current. The difference of the DC-link voltage command and the measured value is fed to a proportional-integral (PI) controller to generate the magnitude I_g of the grid current command, which is multiplied by the unit sinusoidal function with the phase θ of the grid voltage u_g to produce the current command i_g^*. The digital phase-lock-loop (PLL) is used to obtain the phase information [31]. In the inner loop, the difference between the current reference and measured current is provided as the input of another PI controller. The output of the PI controller is compared with the triangle carrier waveform to generate the gate signals for the full-bridge converter.

A feedforward compensator is added to the output of the current controller to improve the external disturbance rejection capability and system dynamic performance. The duty ratio D_{rec} of the feedforward compensator can be written as

$$D_{rec} = 1 - \frac{|u_g|}{u_{dc}^*} \tag{1}$$

During a heavy load condition, the DC-link voltage may contain a large voltage ripple with a frequency that is twice the fundamental frequency. This will distort the current reference generated by the outer-loop DC-link voltage controller. Therefore, a low-pass filter (LPF) is needed to attenuate the ripple of the measured DC-link voltage in the outer voltage control loop.

2) Control of DC-DC Converter

Usually the DC-link voltage u_{dc} is higher than that of the battery pack, and the bidirectional DC-DC converter is used as a buck converter. In this paper, the RBP is charged with the CC method, since the battery cells can be charged in a relatively short time with the CC method. A PI controller is used to regulate the duty cycle of the device S_5 to make the charging current to be constant, as shown in Fig. 3. A feedforward compensator is applied to the current control loop.

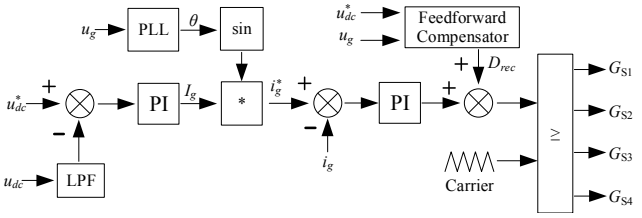

Fig. 2. Control scheme for the AC-DC converter in the G2B mode.

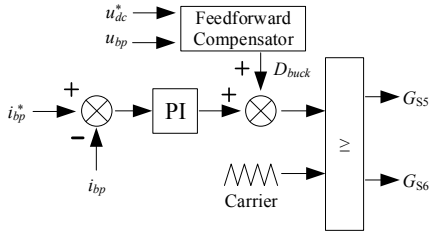

Fig. 3. Control scheme for the DC-DC converter in the G2B mode.

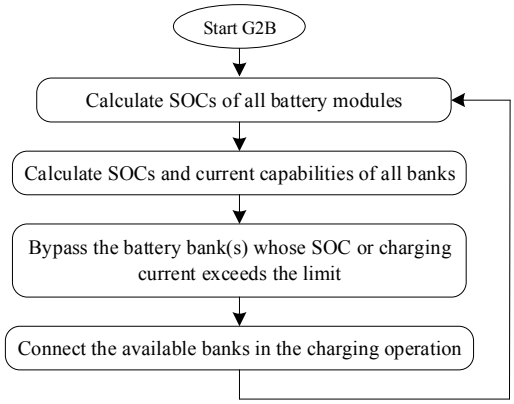

Fig. 4. Operation flowchart of the RBP in the G2B mode.

The duty ratio D_{buck} of the compensator can be expressed as

$$D_{buck} = \frac{u_{bp}}{u_{dc}^{*}} \tag{2}$$

where u_{bp} is the terminal voltage of the RBP, as shown in Fig. 1.

3) Control of RBP

Fig. 6 shows the operation flowchart of the RBP in the G2B mode. Based on the voltage and current of the battery, the SOC balance can be achieved by properly connecting the battery cells and banks using the switching circuit inside the RBP. The SOC of a battery cell can be estimated with the coulomb counting method [30]

$$SOC(t) = SOC(t_0) - \frac{1}{3600Q_0}\int_{t_0}^{t} i(\tau)d\tau \tag{3}$$

where $SOC(t_0)$ is the initial SOC of the battery cell, $i(\tau)$ is the instantaneous charging current flowing through the battery cell, and Q_0 is the rated capacity of the battery cell. Due to the current sensing noise, battery self-discharging effect, battery internal temperature variation, etc., the initial SOC at time t_0 is updated to improve the SOC estimation accuracy by measuring the open circuit voltage (OCV) of the battery cell when the battery cell is under rest for a period of time.

At first, all available battery banks are connected in the circuit to store the energy from the power grid. If the SOC or charging current of a bank reaches or exceeds the maximum limit, respectively, the corresponding bank is cut off from the circuit. The process continues until all of the battery banks are charged. Finally, the SOC equalization is completed.

B. B2G Mode

1) Control of Full-Bridge Converter

In the B2G mode, the full-bridge converter works as a buck inverter for DC-AC power conversion. A single closed current control loop is designed to shape the AC grid current. The grid current reference is determined by the desired power injected into the grid, grid voltage u_g, and phase θ of the grid voltage [32].

A feedforward compensator with the duty ratio D_{rec} described as follows is added to the current control loop

$$D_{inv} = \frac{|u_g|}{u_{dc}^{*}} \tag{4}$$

2) Control of DC-DC Converter

In the B2G mode, the DC-link voltage u_{dc} is provided by the battery pack, and the DC-DC converter is operated as a boost converter. A dual-closed-loop control strategy is designed for the DC-DC converter, where the outer loop controls the DC-link voltage and the inner loop controls the current through the RBP using PI controllers. A feedforward compensator with the duty ratio D_{boost} expressed as follows is used in the outer control loop.

$$D_{boost} = 1 - \frac{u_{bp}}{u_{dc}^{*}} \tag{5}$$

3) Control of RBP

At the beginning of the B2G mode, all available battery banks are connected in the circuit to deliver energy to the power grid. If the SOC or discharging current of a bank reaches or exceeds the limit, respectively, the bank will be disconnected from the circuit. The procedure continues until all of the battery banks are discharged. Eventually, the SOC balance is achieved. Due to the limited voltage boost capability of the buck-boost DC-DC converter, there is a requirement for the minimum number of battery banks to be connected in the circuit to generate the desired DC-link voltage. To reduce this requirement, some DC-DC converters [33] with voltage gains higher than that of the buck-boost converter should be considered.

IV. Experimental Results

A laboratory prototype, as shown in Fig. 5, is constructed to verify the proposed battery system. The key parameters of the prototype are given in Table I. The grid-connected single-phase two-stage bidirectional PWM converter is implemented using three insulated-gate bipolar transistor (IGBT) modules (MG1275S-BA1MM). These modules are driven by the gate driver HCPL-316J. The battery pack consists of 3×2 (i.e., m = 3 and n = 2) lithium-ion battery modules (e.g., B_{11} in Fig. 1) with the nominal voltage of 25.9 V, the capacity of 12.6 Ah, and the power rating 326 Wh. The switches in the RBP are implemented using power MOSFETs (IRFP4668PBF) with the on-resistance of 9.7 mΩ, which are driven by the gate driver ADUM3221ARZ. The switching frequency of the two-stage PWM converter is f_s = 20 kHz. A programmable AC source (Chroma 61512) is used to simulate a power grid. The voltages in the system are sensed by voltage transducers LV20-P. The currents are measured by current transducers CKSR 6-NP. The control schemes are implemented in a Texas Instruments (TI) floating-point DSP TMS320F28335 with a clock frequency of 150 MHz. A 14-bit analog to digital (A/D) converter AD7657BSTZ-ND is used to sample the analog signals. All the analog signals are sampled at the peak of the triangular carriers. The sampling frequency is the same as the switching frequency.

A. G2B Mode

Fig. 6 shows the grid voltage and the phase of the grid voltage estimated using a digital PLL. The zero-crossing

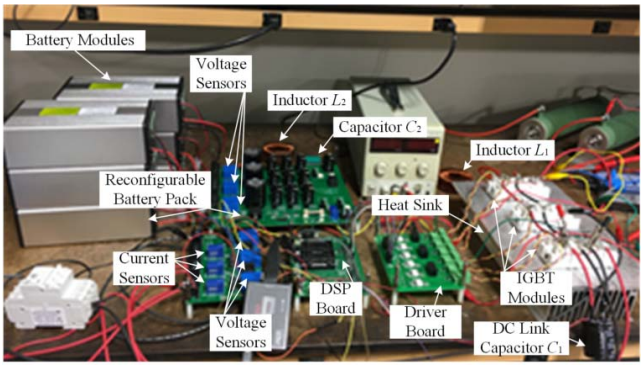

Fig. 5. Laboratory prototype of the proposed grid-tied reconfigurable battery storage system with the test setup.

points of the voltage waveform coincide with the zero points of the estimated phase. Therefore, the PLL tracks the phase of the grid voltage very well in the range between zero and 2π and there is no difference between the estimated phase and the actual phase.

Fig. 7 shows the grid voltage, gate signals of the devices S_2 and S_4, and AC terminal voltage u_{ab} of the AC–DC boost converter in the G2B mode. The amplitude of the emulated grid voltage is 100 V with the line frequency f_g = 50 Hz. The device S_2 is modulated with a switching frequency f_s = 20 kHz while the device S_4 is always off during a positive half-cycle of the grid voltage. The device S_4 is modulated with the same switching frequency while the device S_2 is always off during a negative half-cycle of the grid voltage. It can be seen that the AC terminal voltage u_{ab} has three levels of u_{dc}, 0, and $-u_{dc}$ with the DC-link voltage u_{dc} = 150 V.

Fig. 8 shows the grid voltage and current as well as the charging voltage and current of the battery pack supplied by the two-stage PWM converter in the G2B mode in a steady state. Three, two, and one battery banks are connected in the battery pack for the results shown in Fig. 8(a), (b), and (c), respectively. The THDs of the grid current i_g in Fig. 8(a), (b), and (c) are 2.5%, 3.0%, and 4.2%, respectively, which meet the power quality standard of IEEE 519 that the THD should be less than 5%. The grid current is in phase with the grid voltage, and the PWM converter has the unity power factor. The charging current i_{bp} of the RBP is maintained to be constant at 5.6 A to meet the 2.8 A charging current for each battery module recommended by the manufacturer.

Fig. 9 shows the grid voltage and current as well as the charging voltage and current of the RBP supplied by the two-stage PWM converter in the G2B mode in a dynamic state. The charging process starts with three banks connected in the RBP, as shown in Fig. 9(a). Then, the SOC of one battery

TABLE I:
PARAMETERS OF LABORATORY PROTOTYPE.

Parameter	Value	Parameter	Value
u_g (amplitude)	100 V	L_1	1.2 mH
u_{dc}	150 V	C_1	2200 uF
f_g	50 Hz	L_2	1.5 mH
f_s	20 kHz	C_2	10 uF
i_{bp} (recommend)	5.6 A	B_{ij}	12.6 Ah, 25.9 V

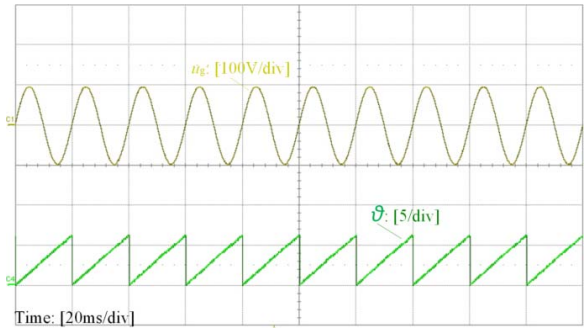

Fig. 6. Grid voltage and estimated phase of the grid voltage.

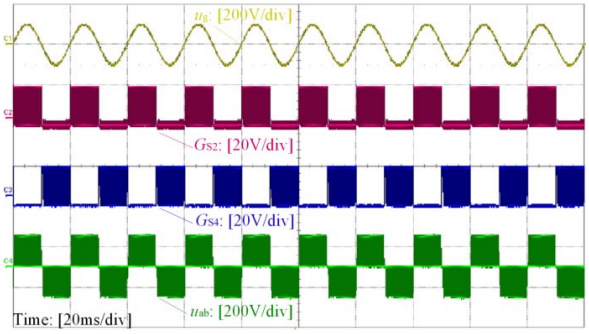

Fig. 7. Grid voltage, gate signals, and AC terminal voltage of the full-bridge converter in the G2B mode.

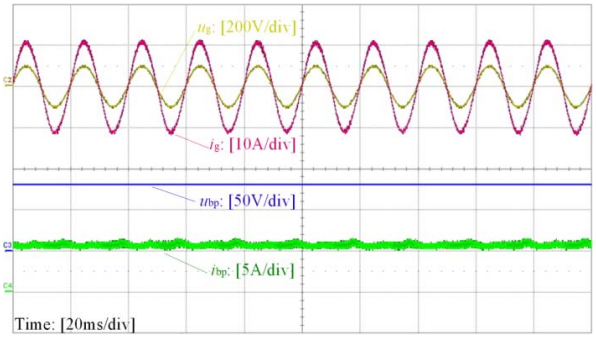

(a)

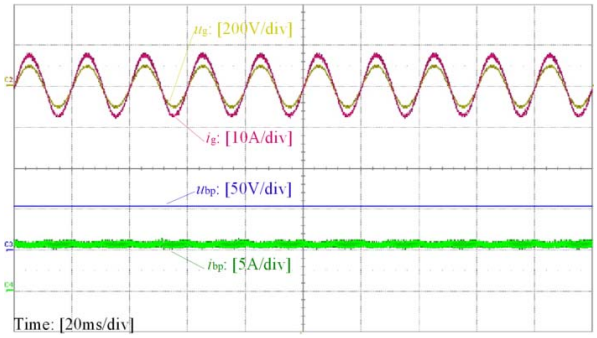

(b)

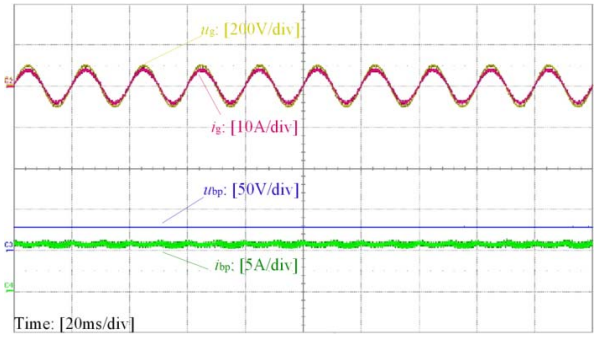

(c)

Fig. 8. Grid voltage and current as well as charging voltage and current of the battery system with: (a) three banks, (b) two banks, and (c) one bank connected in the battery pack.

bank reaches the allowed maximum value. Therefore, the battery bank is bypassed, as shown in Fig. 9(b). Finally, the SOC of another battery bank reaches the maximum value. Therefore, that battery bank is also bypassed, as shown in Fig. 9(c). When one or two banks are bypassed, the remaining bank(s) are still charged to store energy. Eventually, the SOCs of the battery modules are balanced in the G2B mode. At the moment when a battery bank is bypassed, the grid current changes quickly and smoothly; and the charging current of the RBP is controlled to be constant. Therefore, if a battery bank fails, it can be bypassed by the switching circuit quickly without interrupting the operation of the battery system, showing a fault tolerance capability of the battery system.

Fig. 10 shows the SOCs of the three banks in the charging mode. The results clearly show that the battery banks in the charging process are balanced well with the proposed balance control algorithm when the initial SOCs of the three banks are different. A charging limit is set in the G2B mode to avoid overcharge. When the SOC of a battery bank reaches the upper limit, it is bypassed by the switching circuit.

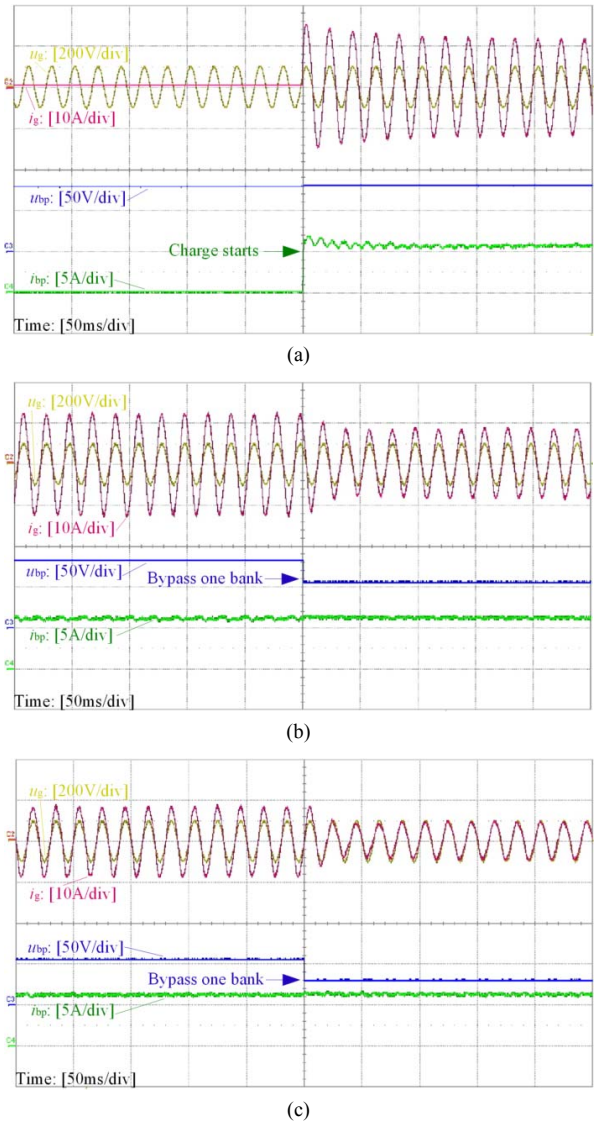

Fig. 9. Grid voltage and current as well as charging voltage and current of the battery system with: (a) three banks, (b) three banks changing to two banks, and (c) two banks changing to one bank in the battery pack.

B. B2G Mode

In the experiment of the B2G operation, a 2.5-kW resistive load with a 5-Ω resistance is connected in parallel with the AC source. The resistive load is necessary in this test because the programmable AC power source cannot absorb the active power generated by the PWM converter.

Fig. 11 shows the grid voltage and current as well as the discharging voltage and current of the battery pack in the B2G mode in a steady state. There are three, two, and one battery banks connected in the pack for the results shown in Fig. 11(a), (b), and (c), respectively. The THDs of the grid current i_g in Fig. 11(a), (b), and (c) have the same value of 2.7%. The grid current is 180° phase shifted from the grid voltage and is maintained to be constant, which is determined by the desired power delivered to the grid. The battery discharging current i_{bp} is changed to satisfy the grid power demand when the terminal voltage of the battery pack varies.

Fig. 12 shows the grid voltage and current as well as the discharging voltage and current of the RBP in the B2G mode in a dynamic state. Before discharge, the battery banks are connected one by one to charge the DC-link capacitor. Then, the discharging process starts with three banks connected in the RBP, as shown in Fig. 12(a). Then, the SOC of one battery bank reaches the allowed minimum value so the bank is bypassed, as shown in Fig. 12(b). Finally, the SOC of another battery bank reaches the allowed minimum value so the bank is also bypassed, as shown in Fig. 12(c). When one or two banks are bypassed, the remaining bank(s) are still discharged to deliver energy. Eventually, the SOCs of the battery modules are balanced in the B2G mode. At the moment when the battery bank is bypassed, the discharging current of the battery pack changes quickly to control the grid current to meet the grid power demand.

Fig. 13 shows the SOCs of the three banks in the discharging mode. The results clearly show that the battery banks are balanced well at the end of the discharging process with the proposed balance control algorithm when SOC imbalance among the three banks occurs. An SOC limit is set

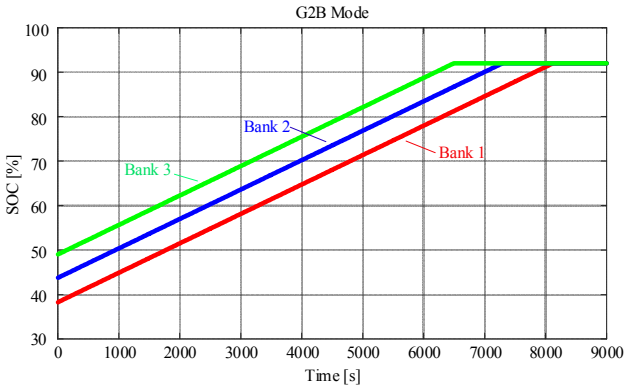

Fig. 10. SOCs of the battery banks in the G2B mode.

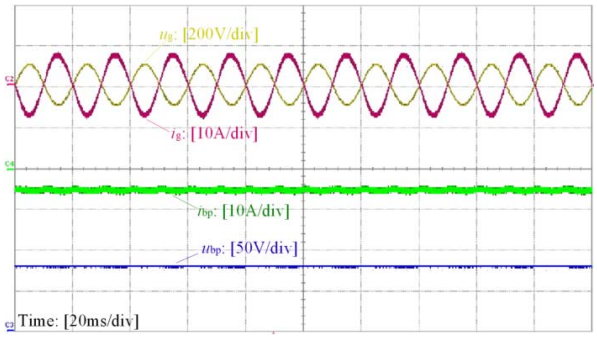

(a)

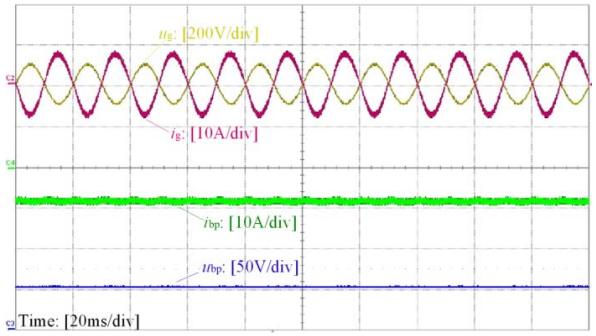

(b)

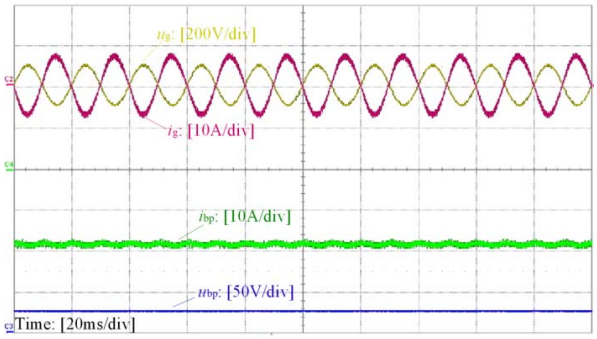

(c)

Fig. 11. Grid voltage and current as well as discharging voltage and current of the RBP with: (a) three banks, (b) two banks, and (c) one bank connected in the battery pack.

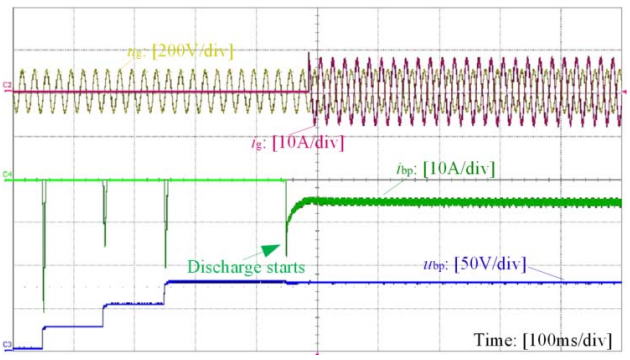

(a)

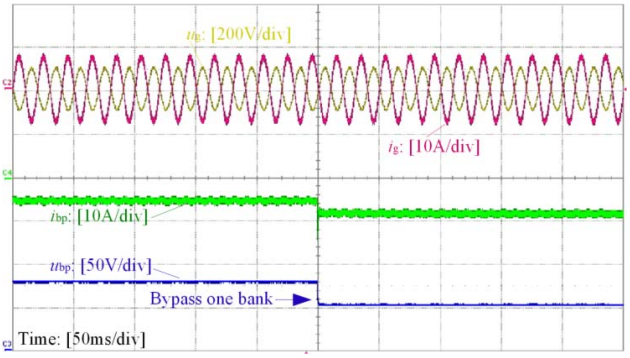

(b)

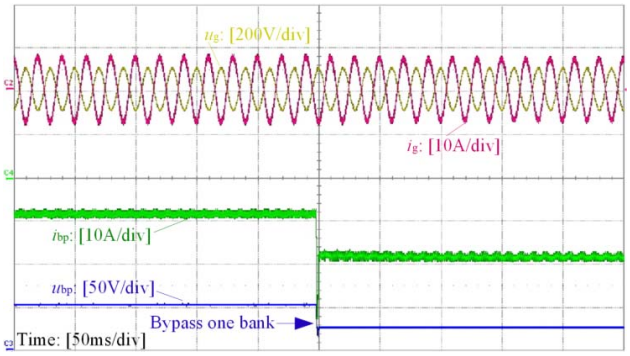

(c)

Fig. 12. Grid voltage and current as well as discharging voltage and current of the RBP with: (a) three banks, (b) three banks changing to two banks, and (c) two banks changing to one bank in the battery pack.

for the B2G mode of operation to extend battery life cycles and avoid overdischarge, because the depth-of-discharge has an impact on the battery lifespan. When the SOC of a battery bank gets to the lower limit, it is bypassed.

V. Conclusion

This paper has presented a grid-tied reconfigurable battery storage system, which consists of a single-phase two-stage bidirectional PWM converter, a RBP, and a central digital control unit that controls the operation mode of the battery system. The circuit configuration, operation principle, and system control schemes were described. Because of the novel switching patterns, the switching loss of the full-bridge converter is reduced compared to the unipolar or bipolar modulation of the converter, and the shoot-through issue of the two semiconductor devices in the same leg is eliminated. With

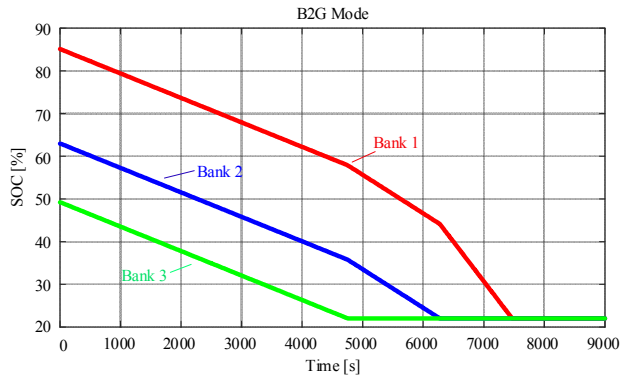

Fig. 13. SOCs of the battery banks in the B2G mode.

the reconfigurable feature of the RBP, the SOC balance can be achieved in both the G2B and B2G modes; no extra SOC equalization circuit is required. Moreover, if one or more battery cells or modules failed, they can be disconnected from the battery pack by the switching circuit quickly without interrupting the system operation, which enabled the fault-tolerance capability and improved the system reliability. With the proposed closed-loop control schemes, the AC grid current has a low THD and unity power factor. A prototype with lithium-ion battery modules was constructed. Experimental results on the prototype validated the aforementioned features of the proposed battery storage system.

REFERENCES

[1] S. M. Lukic, J. Cao, R. C. Bansal, F. Rodriguez, and A. Emadi, "Energy storage systems for automotive applications," *IEEE Trans. Ind. Electron.*, vol. 55, no. 6, pp. 2258-2267, Jun. 2008.

[2] A. Emadi, Y. J. Lee, and K. Rajashekara, "Power electronics and motor drives in electric, hybrid electric, and plug-in hybrid electric vehicles," *IEEE Trans. Ind. Electron.*, vol. 55, no. 6, pp. 2237–2245, Jun. 2008.

[3] S. Vazquez, S. M. Lukic, E. Galvan, L. G. Franquelo, and J. M. Carrasco, "Energy storage systems for transport and grid applications," *IEEE Trans. Ind. Electron.*, vol. 57, no. 12, pp. 3881–3895, Dec. 2010.

[4] M. Bragard, N. Soltau, S. Thomas, and R. W. De Doncker, "The balance of renewable sources and user demands in grids: Power electronics for modular battery energy storage systems," *IEEE Trans. Power Electron.*, vol. 25, no. 12, pp. 3049–3056, Dec. 2010.

[5] A. Khaligh and Z. Li, "Battery, ultracapacitor, fuel cell, and hybrid energy storage systems for electric, hybrid electric, fuel cell, and plug in hybrid electric vehicles: State of the art," *IEEE Trans. Vehicular Technology*, vol. 59, no. 6, pp. 2806-2814, Jul. 2010.

[6] H. Zhou, T. Bhattacharya, D. Tran, T. S. T. Siew, and A. M. Khambadkone, "Composite energy storage system involving battery and ultracapacitor with dynamic energy management in microgrid applications," *IEEE Trans. Power Electron.*, vol. 26, no. 3, pp. 923–930, Mar. 2011.

[7] H. Qian, J. Zhang, J.-S. Lai, and W. Yu, "A high-efficiency grid-tie battery energy storage system," *IEEE Trans. Power Electron.*, vol. 26, no. 3, pp. 886–896, Mar. 2011.

[8] B. Zhao, X. Zhang, and J. Chen, "Integrated microgrid laboratory system," *IEEE Trans. Power Syst.*, vol. 27, no. 4, pp. 2175–2185, Nov. 2012.

[9] M. Yilmaz and P. T. Krein, "Review of battery charger topologies, charging power levels, and infrastructure for plug-in electric and hybrid vehicles," *IEEE Trans. Power Electron.*, vol. 28, no. 5, pp. 2151–2169, May 2013.

[10] D. Boroyevich, I. Cvetkovic, R. Burgos, and D. Dong, "Intergrid: A future electronic energy network?," *IEEE J. Emerging Sel. Topics Power Electron.*, vol. 1, no. 3, pp. 127–138, Sept. 2013.

[11] S. Bai and S. M. Lukic, "Unified active filter and energy storage system for an MW electric vehicle charging station," *IEEE Trans. Power Electron.*, vol. 28, no. 12, pp. 5793–5803, Dec. 2013.

[12] T. Dragicevic, X. Lu, J. Vasquez, and J. Guerrero, "DC microgrids–Part II: A review of power architectures, applications and standardization issues," *IEEE Trans. Power Electron.*, vol. 31, no. 5, pp. 3528–3549, May 2016.

[13] N. Tashakor, E. Farjah, and T. Ghanbari, "A bidirectional battery charger with modular integrated charge equalization circuit," *IEEE Trans. Power Electronics*, vol. 32, no. 3, pp. 2133-2145, Mar. 2017.

[14] E. Chatzinikolaou and D. J. Rogers, "A comparison of grid-connected battery energy storage system designs," *IEEE Trans. Power Electron.*, vol. 32, no. 9, pp. 6913–6923, Sep. 2017.

[15] F. Chen, W. Qiao, and L. Qu, "A modular and reconfigurable battery system," in *Proc. IEEE Appl. Power Electron. Conf. Expo.*, Mar. 2017, pp. 2131-2135.

[16] F. Chen, W. Qiao, and L. Qu, "A scalable and reconfigurable battery system," in *Proc. Int. Symposium on Power Electron. for Distrib. Gen. Syst.*, Apr. 2017, pp. 1-6.

[17] D. Costinett, K. Hathaway, M. U. Rehman, M. Evzelman, R. Zane, Y. Levron, and D. Maksimovic, "Active balancing system for electric vehicles with incorporated low voltage bus," in *Proc. IEEE Appl. Power Electron. Conf.*, Mar. 2014, pp. 3230–3236.

[18] Y. Ye, K. W. E. Cheng, Y. C. Fong, X. Xue, and J. Lin, "Topology, modeling and design of switched-capacitor-based cell balancing systems and their balancing exploration," *IEEE Trans. Power Electron.*, vol. 25, no. 12, pp. 4444–4454, Jun. 2017.

[19] N. Mukherjee and D. Strickland, "Control of second-life hybrid battery energy storage system based on modular boost-multilevel buck converter," *IEEE Trans. Ind. Electron.*, vol. 62, no. 2, pp. 1034–1046, Feb. 2015.

[20] W. Huang and J. A. A. Qahouq, "Energy sharing control scheme for state-of-charge balancing of distributed battery energy storage system," *IEEE Trans. Ind. Electron.*, vol. 62, no. 5, pp. 2764–2776, May. 2015.

[21] Z. Zhang, Y. Cai, Y. Zhang, D. Gu, and Y. Liu, "A distributed architecture based on micro-tank modules with self-reconfiguration control to improve the energy efficiency in the battery energy storage system," *IEEE Trans. Power Electron.*, vol. 31, no. 1, pp. 304–316, Jan. 2016.

[22] Y. Li and Y. Han, "A module-integrated distributed battery energy storage and management system," *IEEE Trans. Power Electron.*, vol. 31, no. 12, pp. 8260–8270, Dec. 2016.

[23] K. Lo, Y. Chen, and Y. Chang, "Bidirectional single-stage grid-connected inverter for a battery Energy storage system," *IEEE Trans. Ind. Electron.*, vol. 64, no. 6, pp. 4581–4590, Jun. 2017.

[24] M. Tolbert, P. F. Zheng, T. Cunnyngham, and J. N. Chiasson, "Charge balance control schemes for cascade multilevel converter in hybrid electric vehicles," *IEEE Trans. Ind. Electron.*, vol. 49, no. 5, pp. 1058–1064, Oct. 2002.

[25] I. Trintis, S. M. Nielsen, and R. Teodorescu, "A new modular multilevel converter with integrated energy storage," in *Proc. 37th Ann. Conf. IEEE Ind. Electron.*, Nov. 2011, pp. 1075–1080.

[26] M. Vasiladiotis and A. Rufer, "Analysis and control of modular multilevel converters with integrated battery energy storage," *IEEE Trans. Power Electron.*, vol. 30, no. 1, pp. 163–175, Jan. 2015.

[27] J. I. Y. Ota, T. Sato, and H. Akagi, "Enhancement of performance, availability, and flexibility of a battery energy storage system based on a modular multilevel cascaded converter (MMCC-SSBC)," *IEEE Trans. Power Electron.*, vol. 31, no. 4, pp. 2791–2799, Apr. 2016.

[28] D. Dong, I. Cvetkovic, D. Boroyevich, W. Zhang, R. Wang, and P. Mattavelli, "Grid-interface bi-directional converter for residential dc distribution systems—Part one: High-density two-stage topology," *IEEE Trans. Power Electron.*, vol. 28, no. 4, pp. 1655–1666, Apr. 2013.

[29] L. Y. Hung, "A novel reduced switching loss bidirectional AC/DC converter PWM strategy with feedforward control for grid-tied microgrid systems," *IEEE Trans. Power Electron.*, vol. 29, no. 3, pp. 1500–1513, Mar. 2014.

[30] T. Kim, W. Qiao, and L. Qu, "Power electronics-enabled self-X multicell batteries: A design toward smart batteries," *IEEE Trans. Power Electron.*, vol. 27, no. 11, pp. 4723–4733, Nov. 2012.

[31] K. J. Lee, J. P. Lee, D. Shin, D. W. Yoo, and H. J. Kim, "A novel grid synchronization PLL method based on adaptive low-pass notch filter for grid connected PCS," *IEEE Trans. Ind. Electron.*, vol. 61, no. 1, pp. 292–301, Jan. 2014.

[32] M. Pahlevani, S. Eren, J. M. Guerrero, and P. Jain, "A hybrid estimator for active/reactive power control of single-phase distributed generation systems with energy storage," *IEEE Trans. Power Electron.*, vol. 31, no. 4, pp. 2919-2936, Apr. 2016.

[33] M. Forouzesh, Y. P. Siwakoti, S. A. Gorji, F. Blaabjerg, and B. Lehman, "Step-up DC–DC converters: A comprehensive review of voltage boosting techniques, topologies, and applications," *IEEE Trans. Power Electron.*, vol. 32, no. 12, pp. 9143-9178, Dec. 2017.